Liquid Crystals
Publication details, including instructions for authors and subscription information:
http://www.informaworld.com/smpp/title~content=t713926090

Model of a disclination core in nematics

Immacolata Sigillo; Francesco Greco; Giuseppe Marrucci

Online publication date: 06 August 2010

To cite this Article Sigillo, Immacolata , Greco, Francesco and Marrucci, Giuseppe(1998) 'Model of a disclination core in nematics', Liquid Crystals, 24: 3, 419 — 425
To link to this Article: DOI: 10.1080/026782998207244
URL: http://dx.doi.org/10.1080/026782998207244

LIQUID CRYSTALS, 1998, VOL. 24, NO. 3, 419–425

Model of a disclination core in nematics

by IMMACOLATA SIGILLO, FRANCESCO GRECO*,
and GIUSEPPE MARRUCCI

Dipartimento di Ingegneria Chimica, Università di Napoli, P.le Tecchio,
80-80125 Napoli, Italy

(*Received 9 June 1997; in final form 8 September 1997; accepted 27 September 1997*)

The core structure of a disclination line of strength +1 in uniaxial nematics is determined by using a space-dependent mean-field approach somehow based on the rod-like molecular model. It is shown that, due to distortion, biaxiality arises at all points of the defect core, except at the centre line where symmetry dictates uniaxiality; the orientational distribution of the rod-like molecules is there 'oblate', however. Although, as is well known, the configuration of a +1 defect is stable only under limiting conditions (as compared with either escaping in the axial direction or splitting into two 1/2 lines), the simple example developed here is indicative of a method which can readily be extended to more realistic, if mathematically more complex, situations such as ±1/2 lines, layers close to solid boundaries, etc.

1. Introduction

Unless special preparation techniques are used, nematic samples usually exhibit a 'polydomain' texture, i.e. a patchwork of nematic regions (domains). At certain points or lines in the polydomain, discontinuities of the director field (see, e.g. reference [1]) are observed, which are the 'defects' of the nematic phase. These discontinuities cannot be dealt with in the context of Frank's theory [2]: in order to gain some understanding of the structure of the defect 'cores', we must resort to a more complex description of the nematic state.

A different approach to non-polar anisotropy was taken long ago by de Gennes [3], in relation to the nematic fluctuations of the isotropic phase close to the nematic transition. In de Gennes' description, the local orientation and degree of order are given by means of a (second rank) order parameter tensor, representing the first significant term of the expansion around isotropy. In later work, the free-energy expression due to de Gennes has also been applied to the nematic state, in particular to determine the core structure of several kinds of defects [4–6]. Of course, since the ground state is no longer isotropic in these cases, the free energy expression due to de Gennes can only be used as an approximation. This point has been discussed elsewhere [7, 8].

A different way of tackling the defect core problem has emerged in recent years, when the availability of high performance computers made it possible to simulate many-body systems. For the case at hand, nematogenic rod-like 'molecules' are packed within a simulation volume, with suitable prescriptions on their orientation at the boundary [9–11]. The system is then made to relax, and the most stable equilibrium configuration is automatically attained. Though straightforward in principle, these simulations remain extremely time consuming, so that only systems made up of a relatively small number of units can be handled, and often some limitations on the degrees of freedom must also be introduced [11]. There is room, therefore, for a different 'molecular' approach, based on distribution functions [12].

More specifically, the molecular organization is described in [12] by means of a space-dependent, one-particle distribution function. Nematogenic interactions are then accounted for at a mean-field level, by suitably generalizing the standard Maier–Saupe expression [13] to a spatially dependent, non-uniform situation. The formulation allows for arbitrarily large distortions of the nematic phase, well beyond the Frank limit, thus encompassing defect cores.

The only defect structure which has been so far explicitly solved by using the distribution function approach is that of the so-called 'hedgehog' point defect [14]. Because of the symmetries of this defect, the nematic phase preserves uniaxiality in the defect core, though the order is strongly modified. The uniaxial character of the distorted nematic in the hedgehog defect is exceptional, however. Distortion-induced biaxiality is expected to be ubiquitous within defect cores [15, 16]. In this paper we report the results obtained with our mean-field approach for the simplest example of biaxial

*Author for correspondence.

molecular arrangement in a defect core, namely that of a line defect of strength +1. We are fully aware that such a defect is rarely encountered in nematics, either because of 'escaping' or because of 'splitting' [17]; a brief discussion on this aspect is postponed to the end of the paper. However, the simple example shown here illustrates the method for future generalizations to other more realistic defect situations.

The paper is organized as follows. A tensorial equation of nematostatics, previously derived [14], is recalled in §2, and particularized to the line defect case in §3, where the relevant boundary conditions are also given. Section 4 reports the results obtained, which are briefly discussed in the last section. Some algebraic details are confined to a short Appendix.

2. Field equation of nematostatics

We use here the simplest model of a nematogenic molecule, which is the rigid rod. Because no internal degrees of freedom are present, the configuration of a rod is given by specifying its position $\mathbf{R}$ and its orientation $\mathbf{u}$. A population of rigid rods is described by means of a space-dependent *orientational* distribution function $f(\mathbf{u}, \mathbf{R})$ which gives the probability density that a rod located at $\mathbf{R}$ is oriented along $\mathbf{u}$. The emphasis on 'orientational' is due to the fact that $\mathbf{R}$ is here seen as a parameter, not as a variable of the distribution. In other words, fluctuations in density are ignored.

All macroscopic observables can be calculated as weighted averages over the distribution function. Of special relevance in what follows is the second order moment $\mathbf{S}$ of the distribution:

$$\mathbf{S} \equiv \langle \mathbf{uu} \rangle \equiv \int \mathrm{d}\Omega f(\mathbf{u}, \mathbf{R}) \mathbf{uu} \tag{1}$$

where $\mathrm{d}\Omega$ is the differential solid angle 'centred' at $\mathbf{u}$. Needless to say, $\mathbf{S}$ generally remains dependent on $\mathbf{R}$. As we shall see, tensor $\mathbf{S}$ is also generally biaxial. In the undistorted equilibrium, however, $\mathbf{S}$ is both constant in space and uniaxial about the director $\mathbf{n}$. As regards the scalar order parameter S, this is unambiguously defined in the uniaxial case only, and it is calculated through the contraction $\mathbf{S}:\mathbf{nn}$. For the distorted biaxial situation, two order parameters are needed, which are linked to the eigenvalues of $\mathbf{S}$.

Tensor $\mathbf{S}$ is sufficient to express the simplest possible generalization of the standard Maier–Saupe potential to distorted situations [12, 14]. The mean-field potential acting at position $\mathbf{R}$ on a rod oriented along $\mathbf{u}$ is given by

$$V(\mathbf{u}, \mathbf{R}) = -kT\, U(\mathbf{S} + l^2 \nabla^2 \mathbf{S}) : \mathbf{uu} \tag{2}$$

where UkT is the potential intensity, and l is a characteristic interaction length, measuring the dimension of the spherical $\mathbf{R}$-neighbourhood whose molecules are 'active' on the test-rod $\mathbf{u}$. {Note that, in the Frank limit, equation (2) corresponds to the one constant approximation. Different mean-field potentials generating three distinct elastic constants can be obtained, at the expense of heavier mathematics, by choosing more realistic shapes of the test-rod neighbourhood [12].}

Because we only deal with equilibrium situations, albeit distorted by defects, the distribution function must be Boltzmannian, i.e. $f \propto \exp(-V/kT)$. We then rewrite equation (1) as:

$$\mathbf{S} = \frac{\int \mathrm{d}\Omega \mathbf{uu} \exp[U(\mathbf{S} + l^2 \nabla^2 \mathbf{S}) : \mathbf{uu}]}{\int \mathrm{d}\Omega \exp[U(\mathbf{S} + l^2 \nabla^2 \mathbf{S}) : \mathbf{uu}]}. \tag{3}$$

[The denominator in equation (3) is the normalization factor of the distribution.] Hence, the equilibrium problem reduces to that of determining the tensor field $\mathbf{S}(\mathbf{R})$ which is the solution of the *functional* self-consistency equation given in equation (3). Of course, suitable boundary conditions must also be prescribed.

The mathematical problem is greatly simplified if the assumption is made that the magnitude of the second term in equation (2) is small, so that $\exp(Ul^2 \nabla^2 \mathbf{S} : \mathbf{uu})$ can be expanded. It should be noted that the assumed smallness of the Laplacian term in (2) should not be confused with the assumption of weak distortions. Indeed, while the latter implies asymptotically small deviations of the eigenvalues of $\mathbf{S}$ from the undistorted situation, the assumption made here only requires that spatial variations are small, with no presumption on the local 'distance' from the undistorted equilibrium. In other words, a truncated expansion of the distribution function is assumed at any point, where the 'ground state' is the local state, whatever the latter may be [8]. When the expansion is made we obtain, after some calculations [14]:

$$\mathbf{S} = \mathbf{P} + Ul^2 (\mathbf{Q} - \mathbf{PP}) : \nabla^2 \mathbf{S} \tag{4}$$

where:

$$\mathbf{P} = \frac{\int \mathrm{d}\Omega \mathbf{uu} \exp(U\mathbf{S} : \mathbf{uu})}{\int \mathrm{d}\Omega \exp(U\mathbf{S} : \mathbf{uu})} \tag{5}$$

$$\mathbf{Q} = \frac{\int \mathrm{d}\Omega \mathbf{uuuu} \exp(U\mathbf{S} : \mathbf{uu})}{\int \mathrm{d}\Omega \exp(U\mathbf{S} : \mathbf{uu})}. \tag{6}$$

Since both tensors **P** and **Q** depend on **S**, equation (4) is a non-linear integro-differential equation for **S** itself. Equation (4) is the general equation of nematostatics, corresponding to the choice made in (2) for the mean-field potential. Needless to say, Maier–Saupe formulation is recovered from equation (4) when considering the undistorted case. On the other hand, highly distorted nematic configurations such as those arising in defect cores (or close to confining walls) can be dealt with by using equation (4).

Let us conclude this section by writing down the expression for the free energy density $a(\mathbf{R})$ in terms of **S**, which will prove useful later in the paper. Calling v the number of molecules per unit volume, the following formula applies [18]:

$$a(\mathbf{R}) = v\left[kT\langle \ln f(\mathbf{u}, \mathbf{R})\rangle + \frac{1}{2}\langle V(\mathbf{u}, \mathbf{R})\rangle \right] \quad (7)$$

where the logarithmic term is the entropic contribution to free energy, and the energetic density (the second term) requires a factor 1/2 because of the mean-field nature of the potential. By substituting equation (2) into (7), and by using again the small gradient approximation, we obtain:

$$a(\mathbf{R}) = vkT\left[-\ln\left(\int \mathrm{d}\Omega \exp(U\mathbf{S}:\mathbf{uu}) \right) + \frac{U}{2}\mathbf{S}:\mathbf{S} + Ul^2\left(\frac{1}{2}\mathbf{S} - \mathbf{P}\right):\nabla^2\mathbf{S} \right] \quad (8)$$

Equation (8) allows one to calculate the free energy density of a nematic sample once tensor **S** has been found from equation (4).

3. Equations for the line defect; boundary conditions

Let us consider a nematic sample inside an infinite cylindrical pipe, whose inner surface has been so treated as to force a strong anchoring of the director in the radial (or else in the tangential) direction (see figure 1). For such a boundary arrangement, and in the absence of escape or splitting, the director field remains radial (or else tangential) up to the pipe axis, where it is undefined, giving rise to the line defect of strength +1 along the axis itself. In the present section we will show how equation (4) specializes for the case of a line defect.

Let us indicate the unit vectors of the cylindrical coordinates as ρ, θ, and **z**. Tensor **S** will then be written as:

$$\mathbf{S} = S_{\rho\rho}\rho\rho + S_{\theta\theta}\theta\theta + S_{zz}\mathbf{zz} + S_{\rho\theta}(\rho\theta + \theta\rho) + S_{\rho z}(\rho\mathbf{z} + \mathbf{z}\rho) + S_{\theta z}(\theta\mathbf{z} + \mathbf{z}\theta). \quad (9)$$

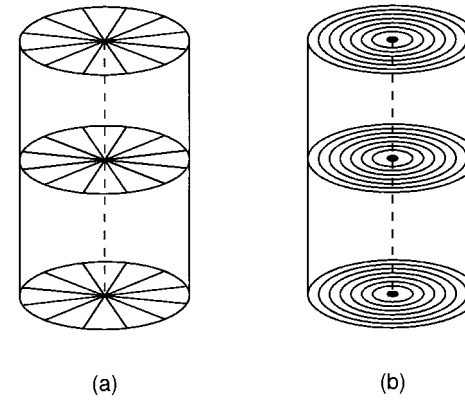

Figure 1. Schematic representation of a +1 line defect (dashed line), with radial (*a*) and tangential (*b*) configurations for the director field.

Implicit in the definition of **S**, equation (1), is a unit trace constraint, which then requires:

$$S_{\rho\rho} + S_{\theta\theta} + S_{zz} = 1. \quad (10)$$

In view of the assumed cylindrical symmetry (no splitting of the defect line), all the components S_{ij} do not depend on θ and z. Thus, we are left with five unknown functions of the radial variable ρ only. However, since escape in the z-direction has been excluded, and our boundary conditions also prevent spiral configurations, the problem is further simplified because the eigenvectors of tensor **S** everywhere coincide with the unit vectors of the cylindrical geometry. We can then write:

$$\mathbf{S} = S_{\rho\rho}(\rho)\rho\rho + S_{\theta\theta}(\rho)\theta\theta + S_{zz}(\rho)\mathbf{zz} \quad (11)$$

so that [recalling equation (10)] the computation of the tensor field **S** is finally reduced to the determination of two scalar functions of the radial variable ρ.

Differential equations for the functions $S_{\rho\rho}(\rho)$ and $S_{\theta\theta}(\rho)$ (say) are readily derived from the general equation of nematostatics, equation (4), in the following way. First, tensor **S** from equation (11) is substituted into (4); the resulting equation is then scalarly multiplied to the dyads $\rho\rho$ and $\theta\theta$, respectively, to obtain:

$$S_{\rho\rho} = P_{\rho\rho} + Ul^2\mathbf{R}:\nabla^2\mathbf{S}; \qquad S_{\theta\theta} = P_{\theta\theta} + Ul^2\mathbf{T}:\nabla^2\mathbf{S} \quad (12)$$

where $P_{\rho\rho} = \mathbf{P}:\rho\rho$, $P_{\theta\theta} = \mathbf{P}:\theta\theta$, and:

$$\mathbf{R} = \mathbf{Q}:\rho\rho - P_{\rho\rho}\mathbf{P}; \qquad \mathbf{T} = \mathbf{Q}:\theta\theta - P_{\theta\theta}\mathbf{P}. \quad (13)$$

In order to obtain explicit expressions for the terms with the Laplacians in equation (12), we exploit: (i) the symmetry of the problem, whereby only the diagonal terms of the tensors **R** and **T** need be considered; (ii) the zero-trace condition of **R** and **T** [easily verified from equations (5), (6), and (13)] whereby only the components

$R_{\rho\rho}$, $R_{\theta\theta}$, $T_{\rho\rho}$, and $T_{\theta\theta}$ can be used. We thus obtain:

$$S_{\rho\rho} = P_{\rho\rho} + Ul^2 \left[(2R_{\rho\rho} + R_{\theta\theta})\nabla^2 S_{\rho\rho} + (R_{\rho\rho} + 2R_{\theta\theta})\nabla^2 S_{\theta\theta} - 2(R_{\rho\rho} - R_{\theta\theta}) \frac{S_{\rho\rho} - S_{\theta\theta}}{\rho^2} \right] \quad (14a)$$

$$S_{\theta\theta} = P_{\theta\theta} + Ul^2 \left[(2T_{\rho\rho} + T_{\theta\theta})\nabla^2 S_{\rho\rho} + (T_{\rho\rho} + 2T_{\theta\theta})\nabla^2 S_{\theta\theta} - 2(T_{\rho\rho} - T_{\theta\theta}) \frac{S_{\rho\rho} - S_{\theta\theta}}{\rho^2} \right]. \quad (14b)$$

Straightforward manipulations (see the Appendix) then lead to the equations

$$\frac{d^2 S_{\rho\rho}}{d\rho^2} = -\frac{1}{\rho}\frac{dS_{\rho\rho}}{d\rho} + \frac{2}{\rho^2}(S_{\rho\rho} - S_{\theta\theta}) + \alpha(U, S_{\rho\rho}, S_{\theta\theta})$$

$$\frac{d^2 S_{\theta\theta}}{d\rho^2} = -\frac{1}{\rho}\frac{dS_{\theta\theta}}{d\rho} - \frac{2}{\rho^2}(S_{\rho\rho} - S_{\theta\theta}) - \beta(U, S_{\rho\rho}, S_{\theta\theta}) \quad (15)$$

where α and β are known functions of $S_{\rho\rho}$ and $S_{\theta\theta}$ (see the Appendix), and ρ has been made non-dimensional by taking the ratio to the interaction length l.

The boundary conditions for equations (15) are as follows. At the capillary wall, i.e. far away from the defect line, we assume the undistorted uniaxial condition, with the principal axis either along the radial or the tangential directions, and the eigenvalues completely specified by the assigned potential strength U. At the defect centre, conversely, the eigenvalues of tensor **S** cannot be assigned beforehand, since their determination is part of the solution itself. The inner boundary condition stems from symmetry alone, which forces the first derivatives to be zero at the cylinder axis. Inspection of equations (15) shows that the zero-derivative condition also prevents the first term on the rhs to diverge at $\rho = 0$.

Further inspection of equations (15) also shows that the difference $S_{\rho\rho} - S_{\theta\theta}$ must approach zero as $\rho \to 0$. Hence, $S_{\rho\rho} = S_{\theta\theta}$ at the line centre, i.e. tensor **S** again becomes uniaxial, this time however with its symmetry axis along the defect line. In between the two uniaxial situations, i.e. the very special one at the centre line and the ordinary one in the far field, we expect tensor **S** to be biaxial.

4. Results

Let us consider the radial defect line, with the director field at the pipe inner surface pointing radially. As already stated, we assume the undistorted state for tensor **S** at the wall. Hence, for any given value of U, the order parameter S at the wall is calculated through the self-consistency condition

$$S = \frac{3}{2}\frac{\int_0^1 dx\, x^2 \exp(USx^2)}{\int_0^1 dx \exp(USx^2)} - \frac{1}{2}. \quad (16)$$

From the order parameter S, the eigenvalues are then calculated as follows: $S_{\rho\rho} = (2S + 1)/3$, and $S_{\theta\theta} = S_{zz} = (1 - S_{\rho\rho})/2$. As regards the boundary condition at the centre of the defect we know that the derivatives of these eigenvalues must be zero.

We also know that $S_{\rho\rho} = S_{\theta\theta}$ at the centre. As regards this condition, two distinct situations can be envisaged, corresponding to either an oblate ('pancake') or prolate ('cigar') shape of the ellipsoid representing tensor **S**. The latter case, however, is expected to be energetically unfavoured since, macroscopically, it would give rise to a defect surface (instead of a defect line) located at that radial position where the director changes from the orientation of the cylinder axis to that in the $\rho\theta$ plane. We thus expect to deal with the oblate case only, which is identified by $S_{zz} < S_{\rho\rho} = S_{\theta\theta}$. This inequality, coupled to the unit trace condition, restricts S_{zz} to the range $S_{zz} < 1/3$.

The set of equations (15), together with the boundary conditions, constitute a *two point boundary value problem*. To find the solution, we adopted a standard technique known as the *relaxation method* [19], which requires initial trial functions for the unknowns. In view of the consideration of the previous paragraph, the trial values of $S_{\rho\rho}$ and $S_{\theta\theta}$ at the centre were taken to satisfy the condition $S_{\rho\rho} = S_{\theta\theta} > 1/3$. In any event, we verified that different choices for the trial functions (with a prolate ellipsoid at the defect centre) did not alter the results of the relaxation procedure, though convergence became significantly slower. We concluded that, at any given U, the solution is indeed unique.

In figure 2, solution of equations (15) for a capillary of radius 20 and for an intensity of the nematogenic potential $U = 7{\cdot}4$ (corresponding to a Maier–Saupe order parameter $S = 0{\cdot}6$) is shown. All three eigenvalues are plotted in figure 2. Moving away from the wall at $\rho = 20$, distortion-induced biaxiality sets in, as shown by the progressive splitting of the eigenvalues $S_{\theta\theta}$ and S_{zz}. A drastic drop in the $S_{\rho\rho}$ value simultaneously occurs in a few units of length (less then 10 from the axis), thus identifying a defect 'core'. In approaching the axis, an 'inversion in biaxiality' takes place, whereby $|S_{\rho\rho} - S_{\theta\theta}|$ becomes smaller than $|S_{zz} - S_{\theta\theta}|$. The value of the S_{zz} order parameter ($S_{zz} = 0{\cdot}26$) which is found at the centre quantifies the expected flattened shape of the **S** tensor ellipsoid (pancake-like): the rod population at the

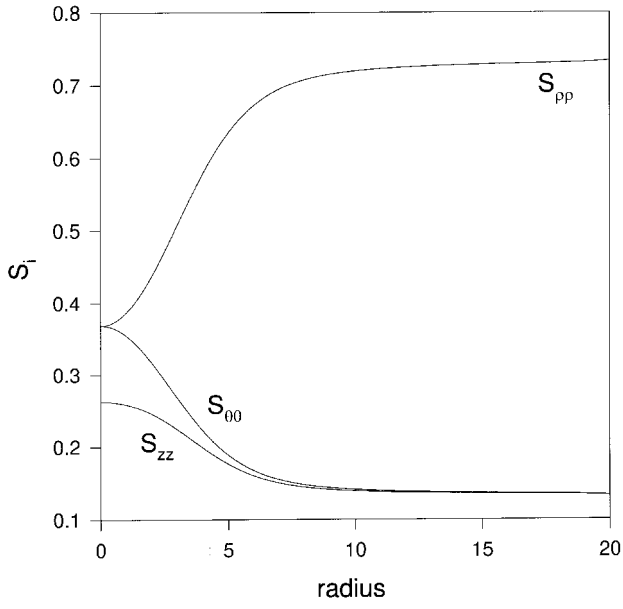

Figure 2. Curves of all three eigenvalues of the order parameter tensor **S** along the radial coordinate (non-dimensional). In kT units, the strength of the Maier–Saupe potential is $U = 7{\cdot}4$.

defect centre is somehow lying down on the $\rho\theta$ plane, isotropically with respect to the z-axis.

Figure 3 depicts the effect of the potential intensity U on the defect structure, for a capillary radius kept fixed at $\rho = 20$. $U = 7$, $U = 7{\cdot}4$, and $U = 8{\cdot}3$ were used, corresponding to increasing values of the equilibrium order parameter at the wall ($S = 0{\cdot}5$, $0{\cdot}6$, and $0{\cdot}7$ respectively).

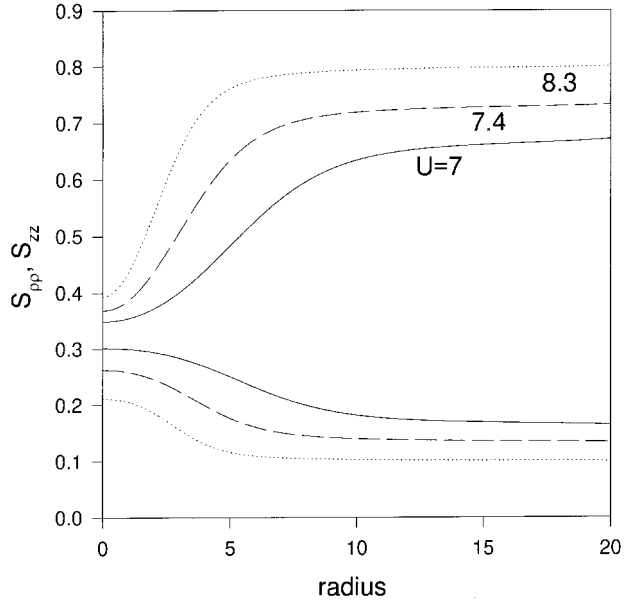

Figure 3. Effect of the strength U of the nematogenic potential on the defect structure. The core size decreases with increasing U.

Inspection of the $S_{\rho\rho}(\rho)$ and $S_{zz}(\rho)$ curves shows that a reduction of the defect size occurs with increasing ordering at the boundary. For the largest U, the wall values of $S_{\rho\rho}$ and S_{zz} persist up to approximately five length units from the axis, i.e. the defect line is essentially confined. Conversely, for the lowest U, a region of constant values close to the wall is no longer recognizable, thus implying that some influence of the defect line spreads radially throughout the sample, and that the Frank elasticity asymptote is not reached anywhere in such a 'small' capillary. Figure 3 also shows that the oblate ellipsoid representing **S** at the defect centre becomes increasingly flat with increasing order parameter at the wall.

Figure 4 reports the non-dimensional free energy density $a(\rho)$ calculated from equation (8) for the same value, $U = 7{\cdot}4$, previously considered (see figure 2). For the sake of comparison, the non-dimensional Frank free energy $a_F = a_0 + US^2/2\rho^2$ is also shown in figure 4, where a_0 is the Maier–Saupe undistorted equilibrium free energy contribution. Several observations should be made here. In the first place, it remains confirmed that in a molecular approach the energy content of a defect line is finite (which removes the Frank elasticity divergence). The molecular approach shows how the nematic order is modified when approaching the defect axis. The general feature is that of a weakening of the nematic order. The spatial distortion modifies the

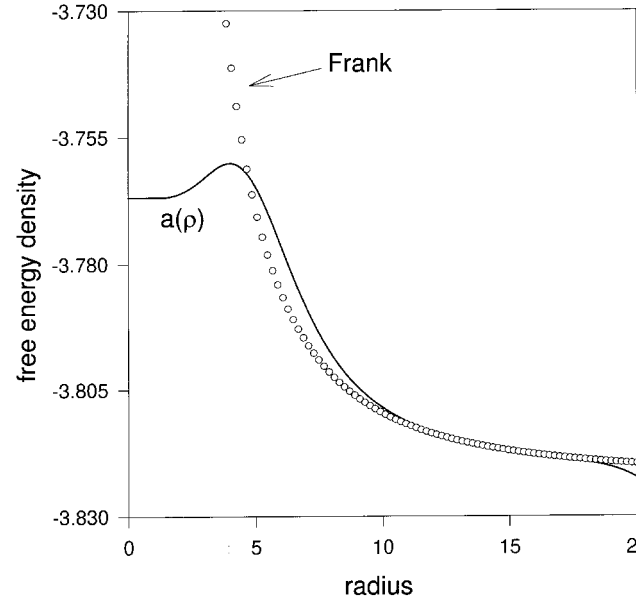

Figure 4. Plot of free energy density versus radial coordinate (non-dimensional), calculated from equation (8) in the text for the case $U = 7{\cdot}4$ (see figure 2). Open dots represent the corresponding Frank free energy, diverging at the defect centre.

molecular orientational distribution, rather than being accumulated without bounds as in Frank elasticity.

A second comment concerns the shape of the computed total free energy curve which, at the defect centre line shows a local minimum, then a maximum in a 'rim' region, finally decaying towards the Maier–Saupe uniform value. This situation can be described loosely in terms of a 'two phase' system, where an ordinary nematic phase 'includes' a weakly ordered central kernel, the interface between them being located at the observed 'rim'. In some sense, this was the original intuitive view of the structure of a defect, where the kernel was assumed to be made up of an isotropic phase [20]. More precisely, our result shows that the energy density close to the axis is that of the local oblate state of the nematic, which of course is different from (and in fact lower than) the energy density pertaining to the isotropic state.

Finally notice that figure 4 confirms the expectation that Frank elasticity should be recovered at some small distance from the centreline. Indeed, in our example the two free energy density curves superimpose from $\rho \approx 10$ onward. The slight separation between the curves observed just at the wall ensues from having imposed the undistorted equilibrium value for the **S** tensor at a finite distance from the axis, whereas such a situation should only be recovered as $\rho \to \infty$. Further calculations for larger capillaries (not reported here) show that indeed the discrepancy at the wall between the two curves disappears with increasing capillary radius.

5. Final remarks

Although all results of the previous section refer to the radial configuration of the line defect, the solution also holds for the tangential configuration if the role of the radial and tangential eigenvalues of tensor **S** is inverted. Indeed, equations (15) still apply as long as $S_{\rho\rho}$ and $S_{\theta\theta}$ are exchanged everywhere (also within the functions α and β), and a similar exchange is made in the boundary condition at the wall; hence the solution remains the same with the two eigenvalues inverted. This situation holds here because, as mentioned previously, the simple potential in equation (2) corresponds to the one constant approximation of Frank elasticity. The results are expected to change for more complex potentials which discriminate between splay and bend.

A point which deserves further comment is the stability problem, in particular with respect to the alternative 'escape in the third dimension' frequently alluded to throughout the paper. In a recent review by Kléman [21] reports of unescaped $+1$ lines are critically examined, and some theoretical justifications for their stability (based on unequal elastic constants) are also advanced. In thin samples of polymeric liquid crystals, unescaped $+1$ lines orthogonal to the bounding surfaces were directly observed, though less numerous than $\pm 1/2$ lines [22]. On the simulation side, Chiccoli *et al.* [11] performed Monte Carlo calculations of a cylindrically confined nematic with homeotropic strong anchoring at the boundary. Although this technique always gives the most stable molecular arrangement, the escaped configuration was never obtained. The explanation of the authors for such a result is that the radius used in the simulations is not large enough. On the basis of our results, we can confirm this conclusion by calculating the free energy per unit length of our defect line, and comparing it with the free energy per unit length of the escaped configuration which is known to be $A = 3\pi K$, with K the elastic constant of the nematic [1]. By expressing K in terms of molecular quantities, starting from the molecular interaction potential given by equation (2) (see ref. [12]), we calculate $A = 6\pi US^2$ (in non-dimensional units). For all cases considered in this paper, these calculations show that the free energy is lower in the presence of the defect line than it would be with the escaped configuration. The smallness of the capillary dimensions for the cases dealt with in this paper should be appreciated, however. Since $l \approx 100$ Å, and $\rho_w = 20$ (see figures 2–4), our capillary radius is $\approx 0{\cdot}2\,\mu$m. Chiccoli *et al.* [11] also give a similar order of magnitude for the capillary radius in their simulations. This state of affairs changes for larger capillaries, because the free energy for the escaped structure stays constant, whereas that of the defect line grows logarithmically with radius.

A final remark concerns the relative simplicity of the approach pursued here, leading to equation (4). The associated numerical calculations are incomparably faster than simulation techniques. All the computations presented in this paper were run on a Pentium PC, and the CPU time required to obtain the curves of the eigenvalues (with a 10^{-3} relative precision) was less than 1 h. It then seems quite feasible to deal with more complex geometries (e.g. $\pm 1/2$ defect lines, where tensor **S** depends on two spatial coordinates), or to generalize equation (4) by allowing for more complex forms of interaction potential than that of equation (2).

Appendix

With reference to equation (14), let us define:

$$\begin{aligned} A_1 &= U(2R_{\rho\rho} + R_{\theta\theta}), & A_2 &= U(R_{\rho\rho} + 2R_{\theta\theta}), \\ A_3 &= -2U(R_{\rho\rho} - R_{\theta\theta}), & B_1 &= U(2T_{\rho\rho} + T_{\theta\theta}), \\ B_2 &= U(T_{\rho\rho} + 2T_{\theta\theta}), & B_3 &= -2U(T_{\rho\rho} - T_{\theta\theta}). \end{aligned} \tag{A1}$$

If B_2 is multiplied throughout to equation (14*a*), and A_2 to equation (14*b*), and a subtraction is made, we

obtain an equation where the only Laplacian term is $\nabla^2 S_{\rho\rho}$. Similarly, by multiplying equation (14 *a*) by B_1, and equation (14 *b*) by A_1, and subtracting, we obtain an equation with only $\nabla^2 S_{\theta\theta}$. To obtain equations (15) in the text, we then only need to divide both those equations by the quantity $D = A_1 B_2 - A_2 B_1$ (which has been numerically verified to be non-zero in all cases). Straightforward algebraic manipulations also give:

$$\frac{A_3 B_2 - A_2 B_3}{D} = \frac{A_3 B_1 - A_1 B_3}{D} = -2 \qquad \text{(A2)}$$

which explains the coefficient of the term $(S_{\rho\rho} - S_{\theta\theta})/\rho^2$ in equations (15). Finally, the functions α and β in equations (15) are defined as:

$$\alpha = \frac{B_2(S_{\rho\rho} - P_{\rho\rho}) - A_2(S_{\theta\theta} - P_{\theta\theta})}{D}$$
$$\beta = \frac{B_1(S_{\rho\rho} - P_{\rho\rho}) - A_1(S_{\theta\theta} - P_{\theta\theta})}{D}. \qquad \text{(A3)}$$

In order actually to perform the numerical calculations, the explicit expressions for the functions $P_{\rho\rho}$, $P_{\theta\theta}$, $R_{\rho\rho}$, $R_{\theta\theta}$, $T_{\rho\rho}$, $T_{\theta\theta}$ are required. These are:

$$P_{\rho\rho} = N_1/g \qquad P_{\theta\theta} = N_2/g$$
$$R_{\rho\rho} = N_3/g - P_{\rho\rho}^2 \qquad R_{\theta\theta} = N_4/g - P_{\rho\rho} P_{\theta\theta} \qquad \text{(A4)}$$
$$T_{\rho\rho} = R_{\theta\theta} \qquad T_{\theta\theta} = N_5/g - P_{\theta\theta}^2$$

where:

$$g = \int_0^1 \mathrm{d}x \int_0^{2\pi} \mathrm{d}\varphi\, E$$
$$N_i = \int_0^1 \mathrm{d}x \int_0^{2\pi} \mathrm{d}\varphi\, f_i E \qquad i \in \{1, 2, \ldots, 5\} \qquad \text{(A5)}$$

and:

$$f_1 = x^2, \qquad f_2 = (1 - x^2)\cos^2\varphi,$$
$$f_3 = f_1^2, \qquad f_4 = f_1 f_2, \qquad f_5 = f_2^2,$$
$$E = \exp\{U[S_{\rho\rho} x^2 + S_{\theta\theta}(1 - x^2)\cos^2\varphi + (1 - S_{\rho\rho} - S_{\theta\theta})(1 - x^2)(1 - \cos^2\varphi)]\}. \qquad \text{(A6)}$$

To derive the expressions above, spherical polar coordinates at any point (ρ, θ, z) within the cylinder were used, with the polar axis parallel to the local unit vector ρ. By calling γ the azimuthal angle between ρ and $\mathbf{u}$, it is $x = \rho\ \mathbf{u} = \cos\gamma$.

References

[1] De Gennes, P. G., 1974, *The Physics of Liquid Crystals* (Oxford: Clarendon Press).
[2] Frank, F. C., 1958, *Discuss. Faraday Soc.*, **25,** 19.
[3] De Gennes, P. G., 1969, *Phys. Lett.*, **30A,** 454.
[4] Schopohl, N., and Sluckin, T. J., 1987, *Phys. Rev. Lett.*, **59,** 2582.
[5] Schopohl, N., and Sluckin, T. J., 1988, *J. Phys. Fr.*, **49,** 1097.
[6] Sonnet, A., Kilian, A., and Hess, S., 1995, *Phys. Rev. E*, **52,** 718.
[7] Katriel, J., Kventsel, G. F., Luckhurst, G. R., and Sluckin, T. J., 1986, *Liq. Cryst.*, **1,** 337.
[8] Greco, F., 1996, *Mol. Cryst. liq. Cryst.*, **290,** 139.
[9] Chiccoli, C., Pasini, P., Semeria, F., and Zannoni, C., 1990, *Phys. Lett.*, **150A,** 311.
[10] Hudson, S. D., and Larson, R. G., 1993, *Phys. Rev. Lett.*, **70,** 2916.
[11] Chiccoli, C., Pasini, P., Semeria, F., Berggren, E., and Zannoni, C., 1996, *Mol. Cryst. liq. Cryst.*, **290,** 237.
[12] Marrucci, G., and Greco, F., 1991, *Mol. Cryst. liq. Cryst.*, **206,** 17.
[13] Maier, W., and Saupe, A., 1958, *Z. Naturforsch.*, **13A,** 564; Maier, W., and Saupe, A., 1959, *Z. Naturforsch.*, **14A,** 882; Maier, W., and Saupe, A., 1960, *Z. Naturforsch.*, **15A,** 287.
[14] Greco, F., and Marrucci, G., 1992, *Mol. Cryst. liq. Cryst.*, **210,** 129.
[15] Lubensky, T. C., 1970, *Phys. Rev. A*, **2,** 2497.
[16] Lyuksyutov, I. F., 1978, *Sov. Phys. JETP*, **48,** 178.
[17] Kléman, M., 1983, *Points, Lines and Walls—In Liquid Crystals, Magnetic Systems and Various Ordered Media* (Chichester: John Wiley).
[18] Priest, R. G., 1973, *Phys. Rev. A*, **7,** 720.
[19] Press, W. H., Flannery, B. P., Teukolsky, S. A., and Vetterling, W. T., 1986, *Numerical Recipes* (Cambridge: Cambridge University Press).
[20] Fan, C., 1971, *Phys. Lett.*, **34A,** 335.
[21] Kléman, M., 1989, *Liq. Cryst.*, **5,** 399.
[22] Shiwaku, T., Nakai, A., Hasegawa, H., and Hashimoto, T., 1990, *Macromolecules*, **23,** 1590.